Catalysis Today xxx (xxxx) xxx–xxx

Contents lists available at ScienceDirect

Catalysis Today

journal homepage: www.elsevier.com/locate/cattod

Stacked wire-mesh monoliths for VOCs combustion: Effect of the mesh-opening in the catalytic performance

Oihane Sanz[a,*], Ezequiel D. Banús[a,1], Aintzane Goya[a], Haizea Larumbe[a], Juan José Delgado[b], Antonio Monzón[c], Mario Montes[a]

[a] Department of Applied Chemistry, Fac. de Ciencias Químicas, University of the Basque Country (UPV/EHU), UFI 11/56, Donostia-San Sebastián, Spain
[b] Materials Science Department, Metallurgical Engineering and Inorganic Chemistry, University of Cádiz, E-11510 Puerto Real, Spain
[c] Department of Chemical and Environmental Engineering, University of Zaragoza, c/P. Cerbuna 12, 50009 Zaragoza, Spain

ARTICLE INFO

Keywords:
VOCs abatement
Pt/OMS-2
Wire-mesh monoliths
Mesh-opening

ABSTRACT

Structured reactors based on low cost metallic wire-mesh substrates of highly enhanced transport properties can be an interesting alternative to parallel channel monolithic reactors. In this work stacked wire-mesh monoliths were studied for volatile organic compounds elimination. Monoliths of different mesh-opening were homogeneously and adherently dip-coated with Pt/Manganese Octahedral Molecular Sieve (OMS-2) bifunctional catalyst. The catalytic activity was tested in toluene and methanol complete oxidation reactions. Catalytic activity increases using stacked wire-mesh monoliths instead of parallel channel monoliths and decreases when increasing the wire-mesh opening, showing the importance of the mass-transfer phenomena (contact between the gas phase and the solid catalyst).

1. Introduction

Volatile organic compounds (VOCs) are classified as major contributor to atmospheric air pollution. Type and nature of VOCs depend on the source of emission. Examples of these pollutants are alcohols, aldehydes, aromatics, alkanes, ketones, olefins, ethers, esters, paraffins, halogenated hydrocarbons and sulfur containing compounds [1]. Several techniques have been proposed for their elimination, being the catalytic oxidation to CO_2, water and other relatively less harmful compounds one of the most effective and inexpensive. One of the main challenges in catalytic VOCs abatement is the selection of the proper catalyst due to variety and nature of VOCs mixtures. Catalyst used for VOCs combustion can be classified into three major groups [1]: (i) noble metals catalyst [2], (ii) non-metallic oxides [2,3] and iii) mixed-metal catalyst [4,5]. In our previous work it has been demonstrated that the Pt/OMS-2 type catalyst is very active for the combustion of aromatic and oxygenated mixture [5]. The manganese octahedral molecular sieve (OMS-2), also called cryptomelane, is a type of manganese oxide that presents very interesting textural properties for platinum dispersion besides its intrinsic activity for the oxidation of VOCs. On this catalyst, they coexist sites as metallic platinum that is able to catalyze oxidation of HCs as toluene, and sites on the manganese oxide surface, where the oxidation of oxygenated compounds like ethyl acetate occurs preferentially.

Conventional catalytic reactors are based on fixed bed catalysts showing several drawbacks, such as a non-homogeneous access to the catalytic surface and a very high-pressure drop. Moreover, VOCs are usually highly diluted in huge streams of end-pipe gases. Under such conditions, catalytic combustion runs in diffusional regime, where reaction rate is limited by the mass transfer between the flowing gas mixture and the catalyst surface. Catalytic systems based on structured substrates are of increasing interest because of the significant improvements they offer in chemical processes, meanly in environmental catalysis and combustion processes [6]. Structured substrates (monoliths [7,8], foams [9–11] meshes [12,13], among others) are three-dimensional structures with channels or macropores that lead to a very low pressure drop and which exhibit high lateral surface where a catalyst thin layer can be applied. Monolithic structured substrates have become one of the most relevant and economically significant applications of catalytic reactor engineering and industrial catalysis so far [6]. However, in recent years open cell foam type structured reactors have been extensively studied in the catalysis field because of the advantages resulting from their structure [9–11,14]. Foams have high pore tortuosity resulting in a turbulent flow as opposed to the laminar flow characteristic of the monoliths with longitudinal parallel channels [15,16]. Turbulence implies better heat and mass transfer properties

* Corresponding author.
E-mail address: oihane.sanz@ehu.eus (O. Sanz).
[1] Permanent address: Instituto de Investigaciones en Catálisis y Petroquímica (INCAPE, FIQ, UNL-CONICET), Santiago del Estero 2829, 3000 Santa Fe, Argentina.

http://dx.doi.org/10.1016/j.cattod.2017.05.054
Received 2 February 2017; Received in revised form 8 May 2017; Accepted 13 May 2017

resulting in a better catalytic performance at the cost of a certain increase in pressure drop [10,17,18]. However, one of the main drawbacks of foams is its high manufacturing cost.

Other interesting structured substrates that combine the excellent mass and heat-transfer characteristics with lower manufacturing cost are metal mesh substrates [19–21]. These types of substrates present 10 times higher mass and heat-transfer coefficient than the parallel channel monoliths [22]. There have been attempts to utilize wire meshes made of cheap iron or stainless steel as structured substrates for different catalytic applications [12,21–24]. Nevertheless, little attention has been paid to the configuration of the wire-mesh substrate. Sun et al. [24] designed wire-mesh honeycombs by alternating corrugated and plain wire-mesh sheets, which combined the characteristics of wire-mesh catalyst and the parallel channel monoliths. Perez-Ramírez et al. [25] described designs of wire gauzes of active metals for industrial applications showing 3D wire configurations (knitted and woven gauzes) as being the more effective. Banus et al. [12] prepared a new type of wire-mesh monoliths that consisted of stacking corrugated wire-mesh discs in metallic cartridge. The stacked wire-mesh monoliths showed better activity for the diesel soot abatement than those present in normal diesel engine exhausts.

The aim of this work is to evaluate the performance of stacked wire-mesh structured substrates for VOCs abatement. Washcoating process was studied to coat structured substrates with the Pt/OMS-2 catalyst. Toluene and methanol were chosen as model molecules to evaluate the effect of the wire-mesh opening in the total catalytic oxidation of VOCs.

2. Experimental

2.1. Construction of structured substrates

Two types of metallic structured substrates made by AISI 304 stainless steel have been used: parallel channel monoliths and stacked wire-mesh monoliths. Both monoliths types were cylindrical (D = 16 mm; L = 30 mm). Homemade parallel channel monoliths consisting of 50 μm sheets corrugated using rollers producing different channel sizes were fabricated (see Table 1). Monoliths were made by rolling around a spindle alternate flat and corrugated sheets. The stacked wire-mesh monoliths were constructed as described in the work of Banús et al. [12]. In a cylindrical cartridge of AISI 304 stainless steel 40 wire-mesh discs were introduced. The discs were cut by blanking which also produced two small transverse indentations by stamping (see Fig. 1). These indentations allow the discs to be 90° alternately stacked with a small gap between them (0.15–0.30 mm), which facilitates the passage of the gases and especially the process of coating with catalyst. The ends of the cartridge are closed by spot welding with two covers made of the same mesh by drawing (Fig. 1). Three types of wire-mesh with different mesh opening were used (see Table 1).

After the structured substrate construction a pretreatment was performed calcining substrates at 900 °C for 1 h in a tubular furnace under synthetic air (10 ml/min, heating rate 10 °C/min) to produce a rough layer that enhanced the adherence of the catalytic coating [26].

2.2. Powder catalyst preparation

In this work a manganese oxide in the form of octahedral molecular sieve (OMS-2, also called cryptomelane) has been synthesized by the reflux method [27]. Briefly, 11 g of $Mn(CH_3COO)_2{\cdot}4H_2O$ (Aldrich) were dissolved in 40 cm^3 of a buffer solution containing 5 ml of glacial acetic acid and 5 g of $K(CH_3COO)$ in 40 cm^3 of deionized distilled water (DDW). To this buffered solution 150 cm^3 of DDW containing 6.5 g of $KMnO_4$ (Aldrich) was added slowly while stirring and further refluxed under continuous stirring for 24 h (pH 4.5). At the end of the synthesis procedure the obtained solid was filtered, washed, dried at 120 °C for 30 min and calcined at 450 °C for 2 h. For the catalyst slurry preparation, the synthesized OMS-2 was used without calcination process. The Pt/OMS-2 catalyst was prepared by adding the desired amount of Pt $(NH_3)_4(OH)_2$ Johnson Matthey to the washcoating slurry which is subsequently dried and calcined.

2.3. Washcoating of structured substrates

The washcoating process of the structured substrates was carried out by dipping and withdrawing the monoliths in the catalyst slurry at constant speed (3 cm/min). For the coating with only OMS-2 the composition of the slurry was: 10 wt.% of OMS-2, 4 wt.% of colloidal alumina Nyacol AL20. For the coating with Pt/OMS-2, 0.15 wt.% Pt $(NH_3)_4(OH)_2$ Johnson Matthey was added to the previous slurry formulation. The effect of slurry pH (2–10) and catalyst particle size on the slurry stability was studied. After coating, the monoliths were centrifuged to eliminate the excess slurry (400 rpm for 2 min). The coating was repeated several times using the same slurry with a drying step at 120 °C for 30 min between coatings to deposit at the end of the process around 250 mg of the catalyst. Finally, coated monoliths were calcined at 500 °C for 2 h.

2.4. Characterization techniques

The rheological properties of the slurries were measured in a rotational viscometer TA Instruments AR 1500ex at 298 K, the viscosity values at 3400 cm^{-1} shear rate were taken into account. The Zeta Potential was measured using a MALVERN Zetasizer 2000 instrument. Solids were dispersed in an aqueous solution of 1 mM NaCl. The pH of the solutions was adjusted with HNO_3 or NH_4OH solutions. Particle size distribution of the catalyst was measured with a Laser Particle Size Analyzer MALVERN Master Sizer 2000.

The catalytic coating quality was evaluated by different techniques. On the one hand, the adherence of the catalytic layer deposited onto structured substrate was evaluated using an ultrasonic technique by

Table 1
Geometric characteristics of the structures substrates prepared.

Monolith type	Stacked wire-mesh monolith			Parallel channel monolith	
	WM1	WM2	WM3	PC1	PC2
	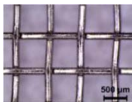	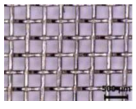	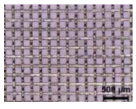	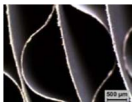	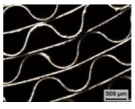
Wire diameter (μm)	160	100	60	–	–
Mesh-opening (μm)	530	250	125	–	–
cpi (cells/in.^{2})	–	–	–	290	1380
Geometric surface area (cm^2/monolith)	151	179	198	207	420
Front void fraction (%)	0.59	0.51	0.46	0.91	0.83

Fig. 1. Details of the stacked wire-mesh monoliths construction.

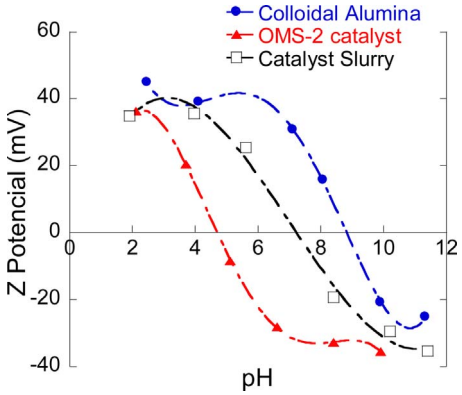

Fig. 2. Zeta potential of the OMS-2 catalyst, colloidal alumina and slurry formulation as a function of pH.

measuring the weight loss caused by exposition to ultrasound [28]. The coated structured substrates immersed in petroleum ether were submitted to ultrasonic treatment for 30 min at room temperature. The results are presented in terms of the retained amount of coating on the structured substrate, expressed as percentage of the initial load. On the other hand, the pressure drop of the monoliths at different gas velocities was measured with a Digitron 2080P Pressure Meter. Finally, the morphology of the surfaces during the different steps of the catalytic substrates preparation was observed by SEM (Hitachi S-2700) and optical microscopy (Leica DFC280).

The size distribution of the Pt nanoparticles was determined by transmission electron microscopy (TEM) using High Angle Annular Dark Field-Scanning Transmission Electron Microscopy (HAADF-STEM). The images were obtained using a FEG-JEOL2010 microscope operated at 200 kV and using a 0.5 nm probe. This technique allows identifying the platinum nanoparticles univocally on the support. In order to obtain representative particle size distributions of the samples, over 250 particles were counted. The same equipment was used to obtain High Resolution Electron Microscopy images. Elemental analyses were conducted by combining the STEM mode with X-EDS detectors (Oxford Inca Energy-200).

Textural properties of the catalysts were determined by nitrogen adsorption using a Micromeritics ASAP 2020. A homemade sample cell that allows analyzing the complete structured substrates was employed. X-ray diffraction (XRD) analysis was performed on a Bruker D8 Advance diffractometer. Diffraction patterns were recorded with Cu Kα radiation over a 5–80° 2θ using a position sensitive detector with a step size of 0.05° and a step time of 5 s. A Micromeritics AutoChem II 2920 instrument was used for temperature-programmed reduction (TPR) experiments (10 °C/min with 10% H_2 in Ar, 25 mg of catalyst).

The catalytic activity of the samples was evaluated by means of the light-off curves of toluene and methanol in air. Complete oxidation reactions were carried out in a tubular fixed-bed reactor at atmospheric pressure and heating rate of 2 °C/min. The light-off curves were obtained at 500 Ncm^3/min of an air stream containing 1000 mgC/Nm^3 of VOCs (toluene or methanol). The catalytic activity of the structured substrates was analyzed by decreasing temperature, avoiding the coupling between the adsorption–desorption phenomena and the catalytic oxidation observed during the temperature increment [29,30]. The temperature of the reactant mixture was continuosly monitored by a thermocouple placed at the inlet of the monolith. Conversion was obtained by measuring the production of CO_2 monitored by an on-line detector (Vaisala GMT220). The yield to CO_2 was calculated as the ratio between the CO_2 concentrations divided by its value measured when complete conversion at high temperature has been reached.

3. Results and discussion

3.1. Catalyst slurry optimization

Washcoating process using catalyst particles suspension is an excellent method to coat wire-mesh structured substrates for different applications [12,22,24]. First of all, the zeta potential was measured as a function of pH to indentify the pH region for optimum dispersion of the OMS-2 catalyst (see Fig. 2) [31]. High zeta potential values of OMS-2 catalyst, indicative of good dispersion, were observed under either a strongly acidic (pH < 4) or a basic (pH > 7) environment. The isoelectric point of the catalyst occurred at pH 4.7. However, the incorporation colloidal alumina (additive necessary to improve the OMS-2 catalyst coating adherence on structured substrate [32]), the isoelectric point shifted to more basic pH, around pH 7.5, below to alumina isoelectric point. High zeta potential values of catalyst slurry were observed under either an acidic (pH < 6) or a strongly basic (pH > 9) environment.

The effect of dispersion medium pH on particle size was also measured (see Fig. 3). The largest particles were obtained at pH close to isoelectric point due to formation of aggregates; in addition, larger particle size was obtained when catalyst slurry with colloidal alumina was prepared. The modification of zeta potential curve and particle size when alumina particles were incorporated to OMS-2 catalyst dispersion suggest that the alumina particles are surrounding the OMS-2 particles. However, to obtain stable slurries and adherent catalytic coating particle size below to 10 μm has been proposed [33,34], being consequently no necessary additional ball milling of the catalyst.

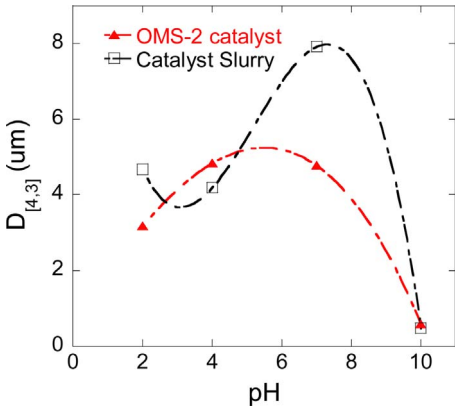

Fig. 3. Particle size of the OMS-2 catalyst and slurry formulation as a function of pH.

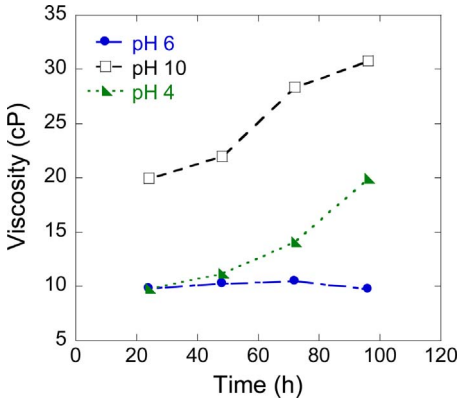

Fig. 4. Evolution of catalyst slurries viscosity prepared at different pH.

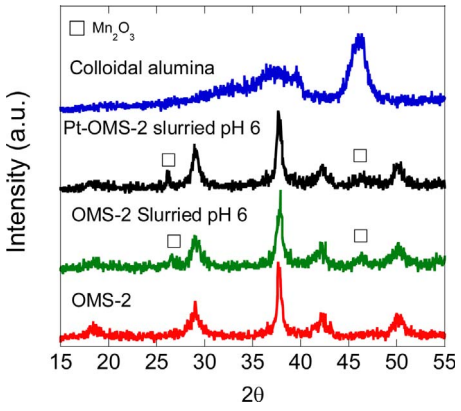

Fig. 5. X-ray diffraction pattern of the powder catalysts.

It has been proposed that the dividing line between stable and unstable suspension is generally taken as zeta potential of ± 30 mV [31]. Therefore, based on zeta potential results (see Fig. 2) three different pH values allowing stable slurries (4, 6 and 10) were selected for catalyst slurry preparation and the evolution of viscosity over time was analyzed (see Fig. 4). The catalyst slurry prepared at pH 10 presents a higher viscosity than the others. Moreover, the viscosity of the slurry at pH 6 kept constant with time, while the viscosities of the other suspensions increased. This indicates that the samples prepared with the highest zeta potential and smallest particle size (see Figs. 2 and 3) present a rheopectic behavior due to the association of the solid particles forming an ordered structure [35].

The adequate viscosity for washcoating to obtain a homogeneous catalytic coating on structured substrates usually ranges between 5 and 30 mPa s (at 3400 s^{-1}) [6]. However, in our previous work we observed that for stacked wire-mesh monoliths coating catalyst slurry viscosity below to 15 mPa s is necessary [12]. Therefore, due to showed stability and viscosity value (9 mPa s), we decided to select pH 6 as the most suitable value to prepare the catalyst slurry for coating.

In addition to a stable catalyst slurry formulation, it is necessary that the coating process does not modify the main catalyst properties: activity, selectivity and stability. That is to say, the methodology used for coating catalyst on structured substrates should not deteriorate the properties of the catalyst. To verify this, the powder catalysts from catalyst slurries (called OMS-2 slurried catalyst) obtained by calcining under the same conditions as the structured catalyst were also characterized. Table 2 summarizes the main textural parameters obtained from nitrogen isotherm: BET surface area (S_{BET}) and total pore volume (V_{PORE}). Slurried catalysts showed higher surface area than OMS-2 catalyst (parent catalyst) due to incorporation of colloidal alumina.

The XRD patterns of powder catalyst are shown in Fig. 5. The main reflections of OMS-2 structure (JVDS 29-1020) at 2θ angles of 18°, 37.5°, 42° and 50° are present. However, in the samples of slurried catalyst (only catalyst slurried at pH 6 is shown) the characteristic peaks of γ-phase of alumina at 2θ 37° and 46° were difficult to identify and two peaks corresponding to Mn_2O_3 (JVDS 41-1442) were also identified at 2θ angles around 26° and 46°. The presence of some α-Mn_2O_3 in the OMS-2 slurried catalyst is also evidenced by H_2-TPR profile (see Fig. 6). For the parent catalyst, the profile is featured by a main reduction peak at about 320 °C, which represents the reduction of MnO_2 to MnO without formation of intermediated Mn_3O_4 [36]. The profile of the OMS-2 slurried catalyst exhibits one more peak around 400 °C related to the reduction of $Mn^{3+} \rightarrow Mn^{2+}$ [37].

Fig. 7 shows toluene light-off curve obtained from the signal of the CO_2 appearance as a function of time for powder samples. It can be seen that the activity of the slurried catalyst undergoes only small modifications at low temperature that disappear when the conversion approaches 100%, being the complete oxidation temperature around 300 °C.

Using the same catalyst slurry formulation at pH 6, 1%Pt-OMS-2 catalyst slurry was also prepared by incorporating platinum precursor into dispersion medium (see Experimental part). The catalyst powder obtained by drying and calcining this slurry (Pt-OMS-2 slurried catalyst) was also characterized. The TPR profile of the Pt-OMS-2 slurried catalyst presented a H_2-consumption peak at much lower temperature than that OMS-2 (see Fig. 6). The peak around 200 °C is attributed to the reduction of PtOX plus the reduction of MnO_2 promoted by spillover of hydrogen species from Pt onto MnO_x [38]. The XRD patterns indicated similar results to the OMS-2 slurried catalyst (see Fig. 5). The OMS-2 structure was preserved after platinum incorporation, some α-Mn_2O_3 was deduced but no peaks corresponding to platinum were observed, suggesting that the metal is highly dispersed on the OMS-2. TEM also provide information regarding Pt particle dispersion (see Fig. 8). Fig. 8A shows a typical STEM-HAADF image of the Pt-OMS-2 catalyst where the platinum particles can be

Table 2
Textural properties of the indicated samples.

Samples		S_{BET} (m^2/g)	V_{PORE} (cm^3/g)
Powder catalyst	OMS-2 catalyst	89	0.43
	OMS-2 slurried pH 4	123	0.50
	OMS-2 slurried pH 6	113	0.44
	OMS-2 slurried pH 10	119	0.43
	Pt/OMS-2 slurried pH 6	120	0.50
	Colloidal alumina	157	0.37
Structured catalyst	OMS-2/PC1	100	0.43
	OMS-2/PC2	109	0.42
	OMS-2/WM1	105	0.44
	OMS-2/WM2	101	0.43
	OMS-2/WM3	103	0.40

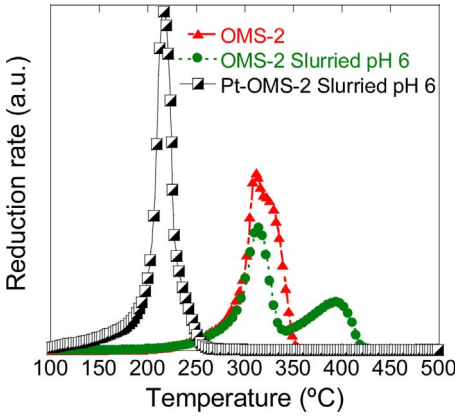

Fig. 6. H_2-TPR profile of the powder catalysts.

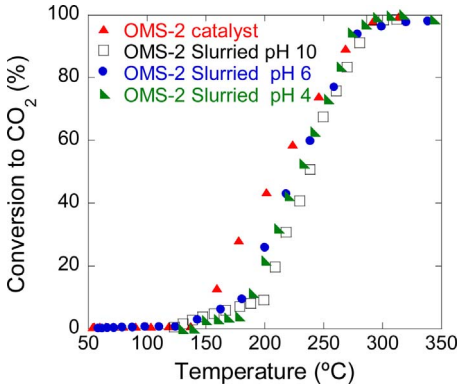

Fig. 7. Toluene ignition curves for powder catalyst.

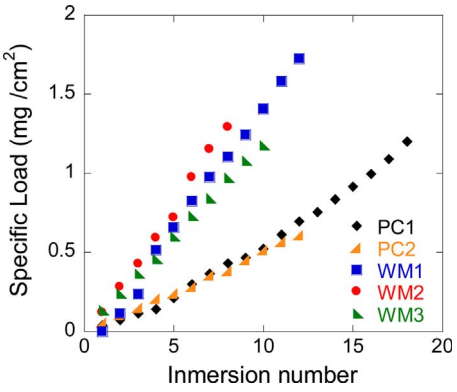

Fig. 9. Specific catalyst load vs. coating cycles for different structured substrates.

distinguished due to bright white contrasts produced the higher Z number of Pt in comparison with Mn. The platinum particle size distribution was 79% and the average crystallite size was 0.77 nm. It should be pointed out that the OMS-2 morphology is unaffected by the catalyst slurry process (Fig. 8A and B). The OMS-2 fibers exhibit diameters between 10 and 20 nm, showing a preferential growth of the fibers along the [1 1 0] orientation. Additionally, the TEM images show that the OMS-2 fibers are coated by colloidal alumina particles (Fig. 8B–E).

3.2. Washcoating of structured substrates

In Fig. 9, the amount of catalyst loaded over the substrates is plotted versus the number of coatings. It is shown that the specific load increased almost linearly with the number of coatings. The washcoating method gave additive and homogeneous results. In addition, it can be observed that the stacked wire-mesh monoliths presented a higher specific load than the parallel channel monoliths. This result could be explained by the geometry difference of monoliths. Stacked wire-mesh monoliths present large curvature of the wire surface and many wire intersection points producing accumulations [12].

The optical images of the monoliths coated with approximately 250 mg of OMS-2 catalyst are shown in Fig. 10. The washcoating method allowed coating parallel channel monoliths and stacked wire-mesh monoliths without structure clogging. However, to evaluate the homogeneity inside monoliths requires breaking and opening the structured catalyst completely. In our previous work pressure drop measurement before and after coating process was proposed for coating quality evaluation [12]. The catalyst coating on the metallic mesh can seriously increase this pressure drop by production of heterogeneities and channels plugging. Fig. 11 presents the pressure drop of the structure substrate coated with around 250 mg at different gas velocity. The stacked wire-mesh monoliths presented higher pressure drop than parallel channel monoliths, suggesting higher turbulence. It can be also seen that the pressure drop increased due to the decrease in mesh porosity (see Table 1). However, the pressure drop increment due to catalytic coating was moderate, less than 60% at the highest gas velocities.

After monoliths washcoating and calcination, the adherence test was done. The adherence of the catalytic layers was excellent (≈99%) for parallel channel monoliths and slightly lower for stacked wire-mesh monoliths (above 80%). In the case of parallel channel monoliths, the coating is inside the channels and their concave form helps the adhesion blocking mechanically the coating inside the channels [18]. In contrast, the coating on stacked wire-mesh monoliths is external to the struts making more difficult its adhesion. SEM micrograph of coated WM1 monolith after ultrasonic test shows that close to wire intersections there is a zone where most of the coating was lost after the

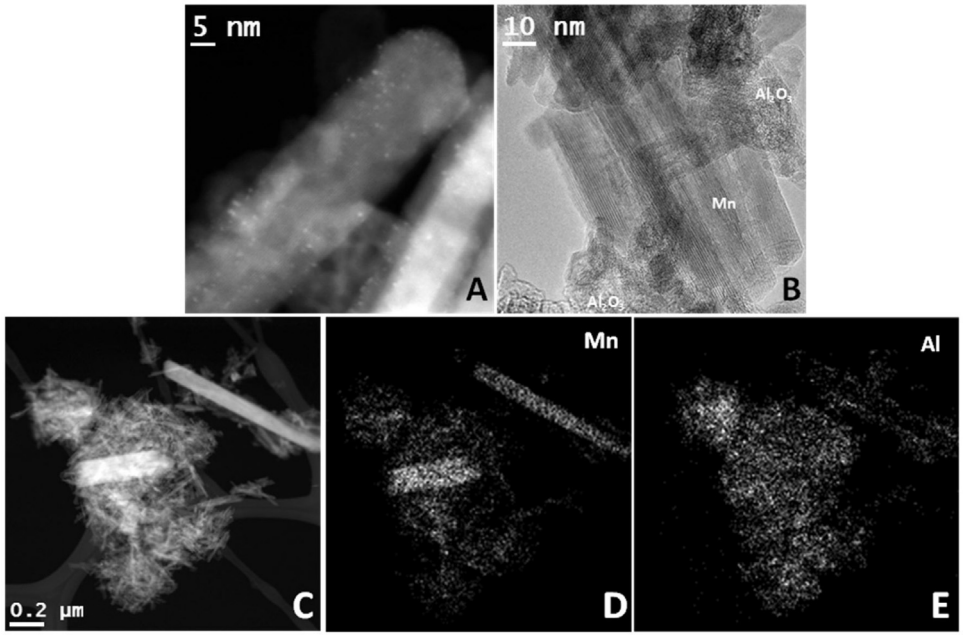

Fig. 8. STEM-HAADF (A, C–E) and HRTEM (B) images of Pt/OMS-2 catalyst.

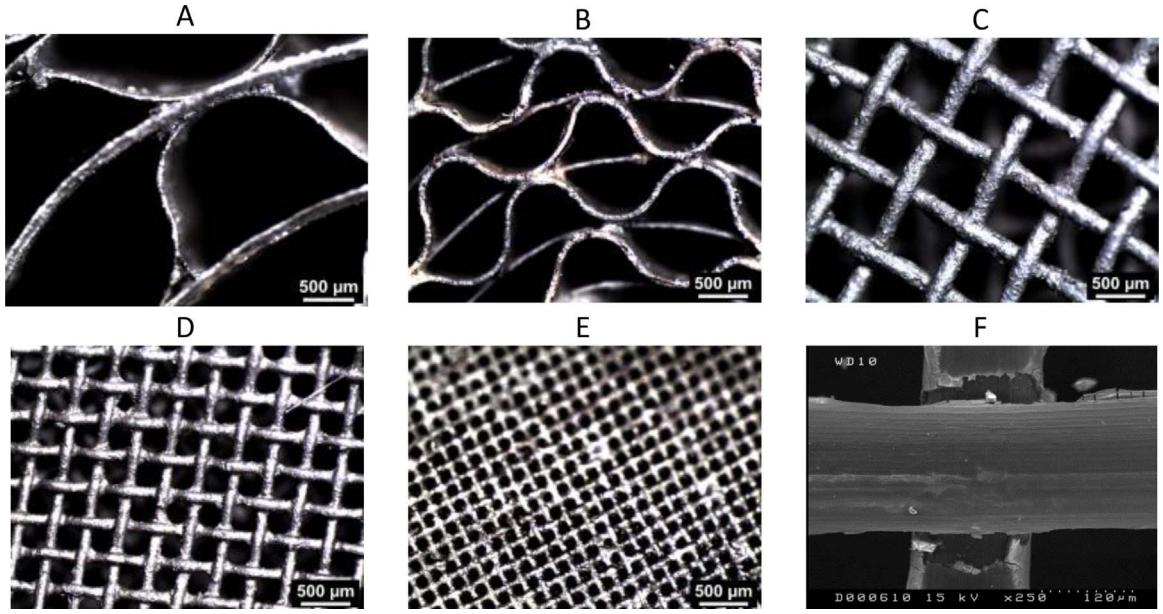

Fig. 10. Images of the coated monoliths: (A) OMS-2/PC1, (B) OMS-2/PC2, (C) OMS-2/WM1, (D) OMS-2/WM2, (E) OMS-2/WM3 and (F) OMS-2/WM1 after adherence test.

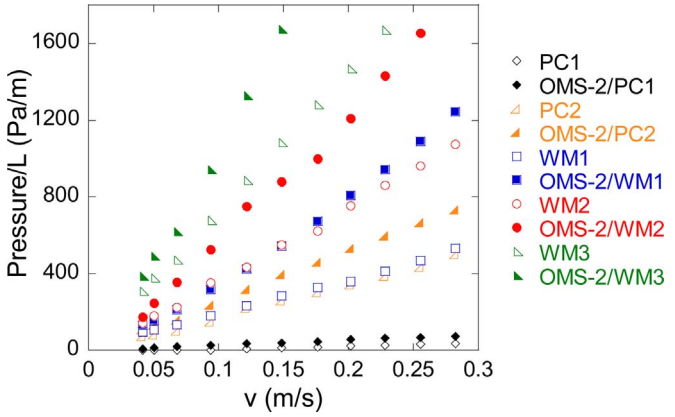

Fig. 11. Pressure drops of the monoliths with and without catalyst coating.

adherence test (see Fig. 10F). On the other hand, the adherence of the catalytic layer increased with the wire-mesh opening (WM1 → 93%; WM2 → 91%; WM3 → 82%). The finer and closer the wires of the mesh are, the lower the adherence of the catalyst is. This result can be explained by the co-occurrence of two factors: larger curvature of the coating on the wire surface and greater number of intersection points between the wires when the wire diameter and mesh opening decreases [12].

3.3. Catalytic performance of structured catalysts

In order to study the effects of the type of structured substrate (parallel channel vs. wire-mesh) and of variation of channel/mesh-opening dimensions for a given loading of catalyst, the series of samples loaded with 250 mg was chosen. The activity for VOCs complete oxidation of the structured catalyst coated with OMS-2 catalyst is considered first. Catalytic tests of toluene and methanol complete oxidation were carried out and the light-off curves (conversion to CO_2 vs. temperature) are presented in Fig. 12. Three main observations can be pointed. Firstly, the stacked wire-mesh monoliths presented higher activity than parallel channel monoliths. Secondly, for the three stacked wire-mesh monoliths, decreasing the mesh-opening increased the catalytic activity. And finally, cell density of parallel channel monolith did not influence the catalytic activity.

Taking into account that all monoliths are coated with similar amount of catalyst, the different activity must be related to the different flow pattern. The better properties of the stacked wire-mesh monoliths as compared with the parallel channel monoliths could be related to a better mixing of reactants due to the tortuosity of the narrow porous substrate structure, resulting in a turbulent flow as opposed to the laminar flow characteristic of the monoliths channels [23,39]. Similar activity improvement was observed comparing foam type structured substrates with parallel channel monoliths for different catalytic applications [10,15–18,40]. These authors attributed this improvement to higher heat transfer and mass transfer of foams. On the other hand, stacked wire-mesh monoliths allowed the preparation of structured catalysts with intermediate properties between fixed beds and monoliths of parallel channels [23,39,41]. These monoliths enhance fluid-catalyst contact at the expense of a moderate increase in the pressure drop [23]. The metal mesh type monoliths are able to enhance the mass transport in the reactors preventing the diffusional limitation of the reaction rate. Łojewska et al. [42] observed that this type of structured reactors allowed dramatic reactor length reductions with a moderate increase in pressure drop comparing parallel channel monoliths.

Our results show also that decreasing the mesh-opening toluene and methanol total combustion temperature decreased in approx 25 °C (see Fig. 12). In this case, the higher activity could be related with turbulence increase when mesh-opening decrease as it was reflected in the pressure drop (Fig. 11). The pressure drop decreases in the series WM3 > WM2 > WM1. Groppi et al. [15,16] reported that mass and heat transfer properties of foams increase with decreasing pore size of the foam (equivalent to mesh-opening). Moreover, Sanz et al. [9] observed that the increase in foam pore density (increase in pore tortuosity) improved effectiveness of the Pt-Al_2O_3 catalyst, requiring lower amount of noble metal for toluene total combustion.

The main conclusion is that in stacked wire-mesh monoliths performance is better due to the higher transfer rates of reactants from the gas phase to the catalytic phase. In the case of the parallel channel monoliths, the impact of the lower mass-transfer rates attained should be much higher. In order to quantify this phenomenon, the apparent activation energy values have been calculated assuming the plug-flow reactor model, and a 1st order kinetics. These calculations allow to detect the presence (or not) of diffusional limitations and their real impact for the parallel channel monoliths and for the stacked wire-mesh monoliths. The results obtained (not shown) clearly indicated that for

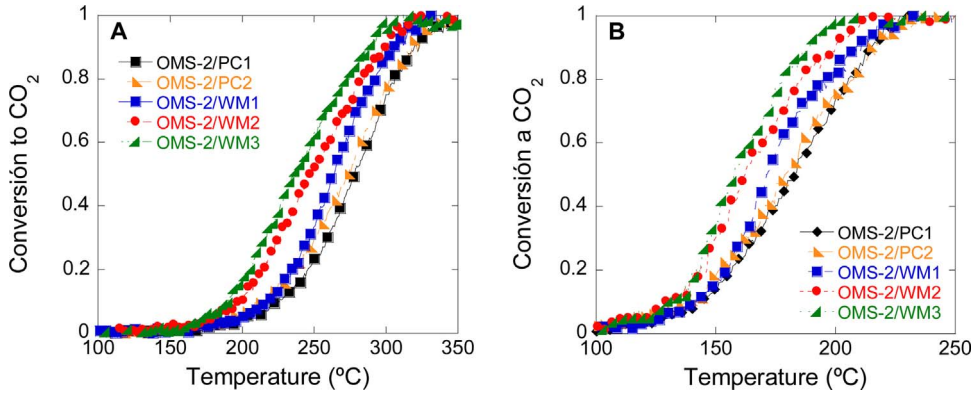

Fig. 12. Toluene (A) and methanol (B) ignition curves.

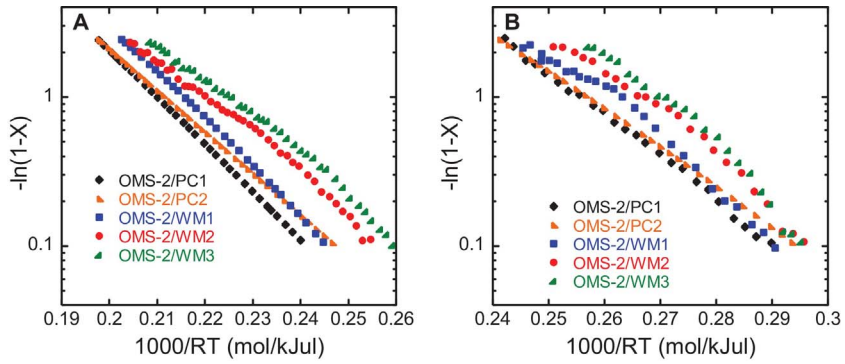

Fig. 13. ln (1-X) vs. 1/RT for monoliths coated with OMS-2 catalyst: (A) toluene and (B) methanol.

the stacked wire-mesh monoliths it is not possible to obtain an appropriate fit of complete conversion-temperature data curve using a unique value of the apparent activation energy. On the contrary, a model that assumes a monotonic decrease of the apparent activation energy decrease along the progress of the reaction fits perfectly the experimental data (not shown). This result is consistent with a transition of the controlling step from the chemical to the diffusional regimen stage. The same kind of conclusions can be obtained directly from the Arrhenius plot (Fig. 13), ln (1-X) vs. 1/RT, where the slope of each curve is the apparent activation energy (E_{app}). In this Figure, it can be seen that the monoliths of longitudinal channels present a relatively constant, and lower valued of the E_{app} than those calculated for the stacked wire-mesh monoliths. Thus, for the mesh monoliths the E_{app} calculated is initially higher (i.e. at low conversion), but this value decreases monotonically as the temperature rises. Therefore, in the mesh monoliths it is observed the change in the control regime from the kinetic to the diffusional one. On the contrary, the lower and constant value of the E_{app} obtained for the monoliths of longitudinal channels, suggest that in this case, the operation is carried out under difusional control. This behavior is consistent with a constant regime controlled by diffusion restrictions. In summary, these calculations confirm our hypothesis that assume a higher performance of the stacked wire-mesh monoliths, as a consequence of a better contact between the reactants, and the catalytic phase deposited on the surface of the wires.

The effect of platinum incorporation in OMS-2 catalyst was also analyzed preparing a series of parallel channel and stacked wire-mesh monoliths. From Fig. 14 it can be observed that the monoliths coated with Pt-OMS-2 were more active than the monoliths coated with OMS-2, and the monoliths geometry presented the same activity trend (MW3 > MW2 > MW1 > PC1 = PC2). Platinum improved the catalytic activity of OMS-2 decreasing the T_{50} and T_{90} toluene oxidation temperatures in around 22 °C for all structured substrates (see Fig. 14A). As concerns the methanol oxidation, OMS-2 with and without platinum showed similar activities that allows oxidizing this VOC at only 195 °C with Pt-OMS-2/WM3 monolith (see Fig. 14). According to our previous work using powder catalyst [5], it seems that for aromatic VOCs the incorporation of platinum onto OMS-2 is beneficial for aromatic compound abatement, being no relevant for oxygenated organic compounds. Toluene combustion takes place preferentially on platinum whereas the methanol on manganese oxide.

Apparently, in VOCs abatement the most important factor affecting the catalyst activity is the geometry of the structured reactor, which it seems to be more important than the incorporation of platinum to OMS-2 (see Fig. 14). The OMS-2/W3M monolith needs 35 °C less than OMS-2/PC1 monolith for methanol or toluene total oxidation. However, the platinum incorporation into OMS-2 decreases toluene oxidation temperature in only 22 °C, producing no changes for methanol oxidation temperatures. The best performance was achieved for the catalysts deposited on the stacked wire-mesh monolith with smaller wire and mesh opening (W3M), playing a major role the mass transfer of reactants to the surface of the catalyst layer.

4. Conclusions

Washcoating procedure was used for coating catalyst layer over two types of metallic monoliths. In this sense, all the structured substrates were successfully coated with OMS-2 and Pt-OMS-2 catalysts in a very uniform and adherent way.

The advantages of the use of structured catalysts based on stacked wire-mesh for the VOCs combustion have been evidenced in this study. The catalytic results show that stacked wire-mesh monoliths present better performance than the parallel channel monoliths. This result suggests that under the conditions studied, the transfer of reactants and products from the bulk gas phase to the catalyst surface, most favored in stacked wire-mesh monoliths, is the controlling step. In addition to that, the decrease in mesh-opening of stacked wire-mesh monoliths produced an increase in the pressure drop, but improves catalytic effectiveness, provably due to the increment of transport rates.

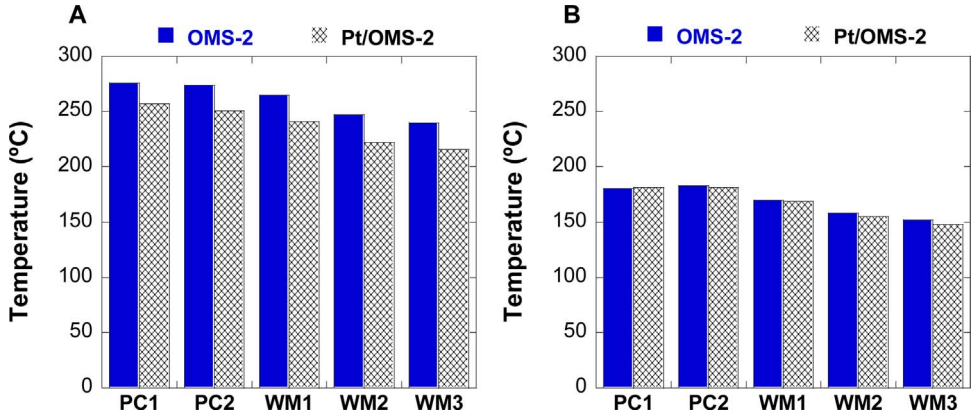

Fig. 14. T_{50} vs. structured catalyst: (A) toluene and (B) methanol combustions temperature.

Acknowledgements

The authors acknowledge the Basque Government (IT1069-16) and the Spanish MINECO/FEDER (ENE2013-47880-C3-1-R, ENE2015-66975-C3-3-R and CTQ2015-73901-JIN) for the financial support. JJD thanks the financial support from the MINECO through the Ramon y Cajal Program and the ATOMCAT project.

References

[1] M.S. Kamal, S.A. Razzak, M.M. Hossain, Atmos. Environ. 140 (2016) 117–134.
[2] C. Lahousse, A. Bernier, P. Grange, B. Delmon, P. Papaefthimiou, T. Ioanidez, X.E. Verykios, J. Catal. 178 (1998) 214–225.
[3] H. Pérez, P. Navarro, G. Torres, O. Sanz, M. Montes, Catal. Today 212 (2013) 149–156.
[4] S. Gangwal, M. Mullins, J. Spivey, P. Caffrey, B. Tichenor, Appl. Catal. 36 (1988) 231–247.
[5] O. Sanz, J.J. Delgado, P. Navarro, G. Arzamendi, L.M. Gandía, M. Montes, Appl. Catal. B: Envriron. 110 (2011) 231–237.
[6] P. Ávila, M. Montes, E.E. Miró, Chem. Eng. J. 109 (2005) 11–36.
[7] J.C. Hernández-Garrido, D. Gaona, D.M. Gómez, J.M. Gatica, H. Vidal, O. Sanz, J.M. Rebled, F. Peiró, J.J. Calvino, Cat. Today 253 (2015) 190–198.
[8] B. Agüero, B.P. Barbero, O. Sanz, F.J.E. Lozano, M. Montes, L.E. Cadús, Ind. Eng. Chem. Res. 49 (2010) 1663–1668.
[9] O. Sanz, F.J. Echave, M. Sánchez, A. Monzón, M. Montes, Appl. Catal. A: Gen. 340 (2008) 125–132.
[10] O. Sanz, L.C. Almeida, J.M. Zamaro, M.A. Ulla, E.E. Miró, M. Montes, Appl. Catal. B: Environ. 78 (2008) 166–175.
[11] F. Ribeiro, J.M. Silva, E. Silva, M. Fátima Vaz, F.A.C. Oliveira, Cat. Today 176 (2011) 93–96.
[12] E.D. Banús, O. Sanz, V.G. Milt, E.E. Miró, M. Montes, Chem. Eng. J. 246 (2014) 353–365.
[13] P.M. Kouotou, G.-F. Pan, S.-B. J.-J.Weng, Z.-Y. Fan, Ind. Tian, J. Ind. Eng. Chem. 35 (2016) 253–261.
[14] S.T. Kolaczkowski, S. Awdry, T. Smith, D. Thomas, L. Torkuhl, R. Kolvenbach, Catal. Today 273 (2016) 221–233.
[15] L. Giani, G. Groppi, E. Tronconi, Ind. Eng. Chem. Res. 44 (2005) 4993–5002.
[16] L. Giani, G. Groppi, E. Tronconi, Ind. Eng. Chem. Res. 44 (2005) 9078–9085.
[17] F.J. Méndez, O. Sanz, M. Montes, J. Guerra, C. Olivera-Fuentes, S. Curbelo, J.L. Brito, Cat. Today 289 (2017) 151–161.
[18] L.C. Almeida, F.J. Echave, O. Sanz, M.A. Centeno, G. Arzamendi, L.M. Gandía, E.F. Sousa-Aguiar, J.A. Odriozola, M. Montes, Chem. Eng. J. 167 (2011) 536–544.
[19] K.-S. Chung, Z. Jiang, B.-S. Gill, J.S. Chung, Appl. Catal. A: Gen. 237 (2002) 81–89.
[20] Y. Matatov-Meytal, M. Sheintuch, Appl. Catal. A: Gen. 231 (2002) 1–16.
[21] A.V. Porsin, A.V. Kulikov, V.N. Rogozhnikov, A.N. Serkova, A.N. Salanov, K.I. Shefer, Catal. Today 273 (2016) 212–220.
[22] A. Kołodziej, J. Łojewska, Catal. Today 105 (2005) 378–384.
[23] P.J. Jodłowski, J. Kryca, M. Iwaniszyn, R. Jędrzejczyk, J. Thomas, A. Kołodziej, J. Łojewska, Catal. Today 216 (2013) 276–282.
[24] H. Sun, Y. Zhang, X. Quan, S. Chen, Z. Qu, Y. Zhou, Catal. Today 139 (2008) 130–134.
[25] J. Pérez-ramírez, F. Kapteijn, K. Schöffel, J.A. Moulijn, Appl. Catal. B: Environ. 44 (2003) 117–151.
[26] L.M. Martínez, O. Sanz, M.I. Domínguez, M.A. Centeno, J.A. Odriozola, Chem. Eng. J. 148 (2009) 191–200.
[27] J. Luo, Q. Zhang, A. Huang, S.L. Suib, Microporous Mesoporous Mat. 35 (2000) 209–217.
[28] S.Yasaki, Y. Yoshino, K. Ihara, K. Ohkubo, US Patent 5,208,206 (1993).
[29] M. Paulis, L.M. Gandia, A. Gil, J. Sambeth, J.A. Odriozola, M. Montes, App. Catal. B: Environ. 26 (2000) 37–46.
[30] D.M. Gómez, J.M. Gatica, J.C. Hernández-Garrido, M. Cifredo, M. Montes, O. Sanz, J.M. Rebled, H. Vidala, App. Catal. B: Environ. 144 (2014) 425–434.
[31] C. Agrafiotis, A. Tsetsekou, I. Leon, J. Am. Ceram. Soc. 85 (2000) 1033–1038.
[32] D.M. Frías, S. Nousir, I. Barrio, M. Montes, L.M. Martínez, M.A. Centeno, J.A. Odriozola, Appl. Catal. A: Gen. 325 (2007) 205–212.
[33] C. Agrafiotis, A. Tsetsekou, A. Ekonomakou, J. Mater. Sci. Lett. 18 (1999) 1421–1424.
[34] S. Tanaka, Z. Kato, N. Uchida, K. Uematsu, Am. Ceram. Soc. Bull. 82 (2003) 9301–9303.
[35] M. Larsson, A. Hill, J. Duffy, Annu. Trans. Nord. Rheol. Soc. 20 (2012).
[36] E. McCullagh, J.B. McMonagle, B.K. Hodnett, Appl. Catal. A: Gen 93 (1993) 203–217.
[37] C.H. Zhang, C. Wang, W.C. Zhan, Y.L. Guo, Y. Guo, G.Z. Lu, A. Baylet, A. Giroir-Fendler, Appl. Catal. B: Environ. 129 (2013) 509–516.
[38] R. Wang, J. Li, Catal. Lett. 131 (2009) 500–505.
[39] K.S. Yang, G. Mul, J.S. Choi, J.A. Moulijn, J.S. Chung, Appl. Cat. A: Gen. 313 (2006) 86–93.
[40] J.T. Richardson, M. Garrait, J.-K. Hung, Appl. Catal. A 255 (1) (2003) 69–82.
[41] A. Kołodziej, J. Łojewska, M. Jarszynski, A. Gancarczyk, P. Jodlowski, Imt. J. Heat Fluid Flow 33 (2012) 101–108.
[42] J. Łojewska, A. Kołodziej, T. Łojewski, R. Kapica, J. Tyczkowski, Appl. Cat. A: Gen. 366 (2009) 206–211.